

COVER PAGE

Document downloaded by @DAEL

Sun Nov 29 01:56:47 2026
For personal use

When automatic English translation is provided, only the original document is authentic.
The EAA cannot be held responsible of any translation error

Bibliographical reference

Finite Element Modeling of Thermoviscous Acoustics on Adapted Anisotropic Meshes: Implementation of the Particle Velocity and Temperature Variation Formulation, Nicolas Joly, Acta Acustica **vol. 96** (Number 1), 2010, pp. 102-114

DOI
https://doi.org/10.3813/AAA.918261

Acta Acustica united with Acustica
Vol. 96 (2010) 102 – 114

DOI 10.3813/AAA.918261

Finite Element Modeling of Thermoviscous Acoustics on Adapted Anisotropic Meshes: Implementation of the Particle Velocity and Temperature Variation Formulation

Nicolas Joly
Laboratoire d'Acoustique de l'Université du Maine, UMR CNRS 6613, Avenue O. Messiaen, Le Mans cedex 9, France. nicolas.joly@univ-lemans.fr

Summary
The numerical computations of thermoviscous acoustics consist of multi-physics and multiscale modeling, combining acoustic propagation at the wavelength scale and momentum and heat transfers at the scale of boundary layer thicknesses. The coupled linear formulation based upon particle velocity and the temperature variation variables is easily implemented using the finite element method. Because acoustic wavelength and boundary layer thicknesses have very different length scales, anisotropic and adaptive meshing is used to optimize the node distribution on the mesh. When combined, the Finite Element Method using degrees of freedom for particle velocity and temperature variation and anisotropic, adaptive meshing technique give the opportunity for accurate numerical solutions at reasonable computational cost.
In order to show the potential of the method, this numerical procedure is applied to axisymmetrical and bidimensional models, illustrating the ability to compute, for complete devices, both propagation and diffusion processes. The physics of the numerical solution is briefly discussed near the discontinuity of a duct and close to the end of a stack inserted in a resonant cavity.

PACS no. 43.20.-f, 43.20.Hq, 43.20.Ks, 43.20.Mv

1. Introduction

The thermoviscous characteristics of the acoustic fluid involve dissipative and reactive phenomena which were already investigated by Kirchhoff [1]. Accounting for these thermoviscous effects clearly arises when dealing with measurement systems based on acoustical phenomena (first of them acoustical transducers and their calibration) or when a refined description of the field inside the boundary layers is needed, to study MEMS devices (Micro Electro Mechanical Systems), capillary domains or porous materials. The study of nonlinear processes such as acoustic streaming or thermoacoustic effects also needs an accurate computation of thermoviscous acoustics. Such numerous applications motivated extensive work on numerical modeling of acoustics in thermoviscous fluid; some important references of the literature are mentioned below, in relation with the approach used to account for the physics.

The phenomena related to the viscosity and the thermal conduction of the fluid are more significant near the boundaries of the acoustic fluid, inside the acoustical boundary layers, because heat- and momentum-transfers with the surrounding structure are more intensive than in the bulk of the fluid. When considering harmonic solutions, the thermal and viscous diffusion processes are characterized by the thermal and viscous boundary layer thicknesses δ_h and δ_ν, and the acoustic propagation by the wavelength λ [2]:

$$\delta_h = \sqrt{2\zeta/\omega}, \quad \delta_\nu = \sqrt{2\nu/\omega}, \quad \lambda = c/f, \tag{1}$$

where f is the frequency, $\omega = 2\pi f$ the angular frequency, c the adiabatic speed of sound, ξ the thermal diffusivity and ν the shear cinematic viscosity of the thermoviscous compressible fluid. The two boundary layer thicknesses are very similar, because they are linked by the relationship $\delta_\nu/\delta_k = \sqrt{Pr}$ where the Prandtl Number of the fluid $Pr = \nu/\xi$ is of order unity. In contrast, as illustrated in Figure 1 for air ($c = 340\,\mathrm{m/s}$, $\xi = 2.1 \cdot 10^{-5}\,\mathrm{m^2/s}$, $\nu = 1.5 \cdot 10^{-5}\,\mathrm{m^2/s}$), the boundary layer thicknesses are much smaller than the wavelength ($\delta_h, \delta_\nu) \ll \lambda$.

When compared to acoustical propagation, the physics of energy diffusion (heat conduction) and momentum diffusion (shear viscous transfer) has a smaller relative importance when the characteristic length of the domain is large compared to the boundary layer thicknesses. Depending on these different length scales and the application, different models can be used:

Received 19 December 2008,
accepted 15 August 2009.

© S. Hirzel Verlag · EAA

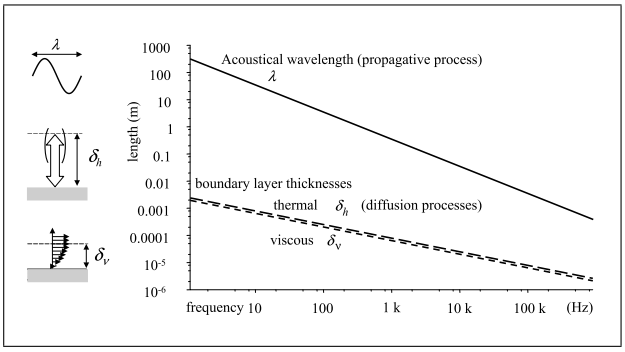


Figure 1. Characteristic length of propagative and diffusive physical processes in thermoviscous compressible air (1bar, 20 °C).

(i) When the boundary layer thicknesses are small compared to the smallest characteristic length L of the domain (δ_h, δ_v) $\ll L$, the thermoviscous effects can be considered as a weak perturbation of the acoustic field that would occur in perfect fluid, i.e. non-viscous and non thermal conducting. The most efficient technique to model such systems in harmonic regime is to adapt the acoustical solution computed in perfect fluid, accounting for the boundary layer effects in using an apparent specific admittance boundary condition for the pressure field [3]. Indeed, due to large wavelength λ and characteristic length L relative to the boundary layer thicknesses (δ_h, δ_v), the total field can be assumed to behave like plane waves near the boundaries. The analytical solution for acoustical, thermal and vortical components [2] gives the local admittance-like boundary condition for the acoustical pressure field. If necessary, the acoustical wavenumber in the bulk of the domain can be corrected according to the dissipative and reactive phenomena developed by thermal diffusion and bulk viscosity. This procedure has been successfully used in both analytical and numerical models [4]: a first computation is performed using a standard numerical code for acoustics in perfect fluid (using for instance the pressure formulation and the Finite Element Method or the Boundary Element Method) with an admittance-like boundary layer β set to an averaged arbitrary value. Since the dissipative phenomena are not accurately accounted for, this first approximate solution may not be precise in amplitude but provides an accurate spatial shape for the acoustic pressure, which allows to compute, on each point of the boundary, the right admittance-like β considering viscous effects ; a second computation involves with the appropriate admittance accounting for thermal and viscous boundary layers effect, and possibly a complex wave number in the bulk of the domain, then gives the precise solution. The admittance-like condition can account for thermal diffusion inside the thick surrounding boundary of the acoustic domain if the isothermal boundary condition for the acoustic fluid is not valid [5],

(ii) When the smallest characteristic length L of the domain geometry is not small compared to the boundary layer thicknesses, the local apparent admittance for thin boundary layers cannot be applied generally. This case includes high curvature geometries or corners (curvature radius at similar or smaller scale than boundary layer thicknesses (δ_h, δ_v)) and capillary domains (whose whole fluid volume is occupied by the boundary layers). Extensive works have been developed in the past decades to study tubes [6, 7], thin layers between parallel surfaces [8, 9, 10, 11, 12], coupling cavities or spherical resonators [13, 14], some of them making use of local analytical solutions to model propagative waves. More recently, numerical methods have been implemented to model, using the Boundary Element Method, heat conducting [15, 16] or viscous fluids [17] using an approximate boundary layer, or using the Finite Element Method in thermoviscous fluid [18, 19, 20, 21, 12] with possibly fluid-structure interaction. The motivation to develop numerical methods arises from the growing demand for computing accurately the thermoviscous acoustic field in a wide range of devices of complex geometry, including corners or composed of subsystems having similar dimensions with the boundary layer thicknesses (δ_h, δ_v).

The modeling of acoustics in thermoviscous fluids is performed in using analytical or numerical solutions. Analytical solutions are obtained in simple geometries from assumptions to be confirmed; numerical solutions can avoid such restrictive assumptions but often lead to high computational cost when dealing with thermal and viscous diffusion at small scale and acoustic propagation at large scale. An efficient and general numerical method is presented in this paper to model thermoviscous acoustics in the above second case (ii), when an equivalent admittance for boundary layers effects cannot be used. This numerical solution can obviously be used to validate the assumptions of analytical models, like the plane-wave approximation used in the first case (i) above. The local acoustic field is considered, in solving the fundamental equations for mass, momentum and energy conservation, meaning that multiphysics is concerned. The characteristic scales of the model are given by the geometry of the fluid domain, but also by the acoustic wavelength and the boundary layer thicknesses (1), such that multiscale modeling including boundary layers is needed. Due to coupled degrees of freedom of multiphysics and refined meshes at the smallest characteristic scale, obtaining an accurate numerical solution for acoustics in thermoviscous fluids can become a challenge. We illustrate in this paper that, taking advantage of complex algebra and using a suitable basic formulation for the physics, the Finite Element Method, when combined with efficient meshing techniques, gives convenient and accurate solutions. A key point is the ability for the recent formulation [5] to be directly implemented in the Finite Element Method. Another one is the use of automatic adaptive and anisotropic meshing techniques, and the efficiency of the presented method results in combining both.

Commercial [22] and open-source [23, 24] multiphysical modeling tools are now available, providing opportunity for full coupled models in a wide range of applications. For a given mesh, such a code may be used to

solve the basic formulation of the problem in using the Finite Element Method. The formulation used below is simple enough to be easily implemented in a Partial Differential Equation solver; for instance, it has been successfully tested [25] with the code Comsol [22]. However, as stated above, another condition for the method is to build a suitable mesh for the physical phenomena to be computed. Most of the multiphysical Finite Element solvers offer capability for creating boundary layer meshes [22, 23]; such commands may be useful to model the acoustic boundary layers, but they are very time-consuming for the end-user to prepare the mesh (because the boundary layer thicknesses (δ_h, δ_v) are frequency-dependant, see Figure 1) and furthermore do not account for the true physical field structure, like local vortices in domains of complicated geometry, that may be far greater or smaller than the boundary layer thicknesses and inconsistent with boundary layers approximations. Retrofit the mesh according to the physics is much more confident for the accuracy of the solution and can exempt the end-user for detailed mesh building. To this aim, it might be possible to use a unique modeling tool like freeFEM [24], but it has not been tested by the author. Isotropic adaptive meshing available in some codes is not adequate because it cannot efficiently fit to the field inside the boundary layers.

This paper presents the procedure to both (i) compute numerically the physical solution for thermoviscous acoustics and (ii) iteratively improve the mesh interpolation. The basic formulation, using particle velocity $\boldsymbol{v}$ and temperature variation τ variables, is reminded in the next section. The numerical solution is performed in implementing this formulation, as presented in section 3 and in appendices for the detailed computation of the Finite Element matrices. A bidimensional anisotropic adaptive meshing technique is introduced in section 4 to retrofit the mesh according to the very different length scales of the total field. To illustrate the potential of the numerical procedure and possible applications, the thermoviscous acoustical field computations of propagative waves in a discontinuous guide (axisymmetrical model) and standing waves in a thermoacoustic device (bidimensional model) are discussed in section 5, before concluding.

2. Basic formulation for linear, harmonic acoustics in thermoviscous fluid at rest

The modeling of thermoviscous fluid is performed according to the following assumptions:

- the length and time scales considered are large compared to the mean free path ℓ and the molecular relaxation time of the fluid particles, such that the continuum mechanics applies. In non monoatomic gases and for frequencies such that relaxation processes cannot be neglected, the physical properties of the fluid have to be modified to equivalent properties depending on the frequency [2],
- the thermoviscous fluid is at rest (no mean movement), Stokesian (viscous stress proportional to rate of strain and heat flux proportional to temperature gradient), and homogeneous ; the physical properties of the fluid are the density ρ_0, the adiabatic speed of sound c, the increase in pressure per unit increase in temperature at constant density $\hat{\beta} = (\partial P/\partial T)_{\rho_0}$, the specific heat ratio γ, the shear μ and bulk η dynamic viscosity and the thermal diffusivity ξ (the cinematic shear viscosity in equation (1) is $\nu = \mu/\rho_0$),
- a small harmonic acoustical perturbation is considered, so that linear approximations remain valid. Using complex algebra and denoting $\mathrm{i} = \sqrt{-1}$, a thermodynamical variable φ_ω describing the small acoustical perturbation at angular frequency ω around some steady state then takes the harmonic form $\varphi_\omega(t) = \Re e\{\varphi \mathrm{e}^{\mathrm{i}\omega t}\}$ and is denoted by its complex amplitude φ. Only the complex variables (pressure variation p, particle velocity $\boldsymbol{v}$, density variation ρ, temperature variation τ) are considered in the following developments, where the time dependence $\mathrm{e}^{\mathrm{i}\omega t}$ and the real part $\Re e\{...\}$ are omitted. The time derivative is then $\mathrm{d}/\mathrm{d}t \approx \partial/\partial t = \mathrm{i}\omega$.

Using these assumptions, some formulations have been proposed to model acoustics in thermoviscous fluids.
The basic equations for mass-, momentum- and energy-conservation may be combined to define some acoustical a, entropic h (thermal) and vortical $\boldsymbol{v}$ (shear movement) components for the total field ($\tau = \tau_a + \tau_h$, $p = p_a + p_h$, $\boldsymbol{v} = \boldsymbol{v}_v + \boldsymbol{v}_a + \boldsymbol{v}_h$) [7, 2, 18, 19], each of these variable satisfying specific equations, and the entropic and vortical components being confined in the boundary layers. The acoustical a and entropic h solutions can be considered in a single equation of higher order, for which the integration needs boundary conditions for derivatives. Another opportunity is to solve directly the full coupled conservation equations using the velocity, pressure and temperature variations [20, 21]. In such models, it is not easy to define the boundary conditions to apply to each of the variables: in the case of a summation $\varphi = \varphi_v + \varphi_a + \varphi_h$, the physical boundary condition usually concerns the total field φ, but the condition on a particular component v, a or h is unknown. Even when considering only total field variables, the boundary condition for the pressure variation p is not obvious: a Dirichlet ($p = 0$ for pressure release) or a Neumann condition ($\partial p/\partial n = 0$ for a rigid boundary in perfect fluid, where $\partial/\partial n = \mathbf{grad} \cdot \boldsymbol{n}$ is the normal derivative) is common in perfect fluids, but inconsistent for accurate conditions on the boundaries of a thermoviscous fluid. Moreover, the use of the pressure variation variable p causes trouble in the interpolation order on the mesh for the different variables [21].

To model acoustics in thermoviscous fluid, there is no need to consider the pressure variation field as a basic variable for the formulation. Accurate modeling of the *viscous* and *thermal* boundary layers rather leads to consider particle velocity $\boldsymbol{v}$ and temperature variation τ. A formulation based upon these variables ($\boldsymbol{v}$, τ) has been proposed [26, 5]: using the fundamental conservation and state equations, the density variation ρ and pressure variation p are

Table I. Thermal and mechanical boundary conditions and symmetry conditions in bidimensional (x, y) or axisymmetrical (r, z) models of thermoviscous acoustics.

Boundary condition	thermal	mechanical
Dirichlet	$\tau = 0$ (isothermal) $\tau = \bar{\tau}$ (prescribed temperature variation)	$\boldsymbol{v} = 0$ (rigid) $\boldsymbol{v} = \bar{\boldsymbol{v}}$ (prescribed velocity)
Neumann	$\partial\tau/\partial n$ (adiabatic)	
x symmetry axis (x, y)	$\partial\tau/\partial y = 0$	$\partial v_x/\partial y = 0$, $v_y = 0$
y symmetry axis (x, y)	$\partial\tau/\partial x = 0$	$v_x = 0$, $\partial v_y/\partial x = 0$
z axisymmetrical axis (r, z)	$\partial\tau/\partial r = 0$	$v_r = 0$, $\partial v_z/\partial r = 0$

expressed in terms of variables $(\boldsymbol{v}, \tau)$

$$\rho = -\frac{\rho_0}{\mathrm{i}\omega}\mathrm{div}\,\boldsymbol{v}, \qquad p = \hat{\beta}\tau - \frac{\rho_0 c^2}{\mathrm{i}\omega\gamma}\mathrm{div}\,\boldsymbol{v}. \tag{2}$$

Substituting for these variations ρ and p in the momentum and energy conservation equations gives the particle velocity and temperature variation formulation

$$\begin{aligned}&\omega^2\boldsymbol{v} + B\,\mathbf{grad}\ \mathrm{div}\,\boldsymbol{v} + C\,\mathbf{curl}\,\mathbf{curl}\,\boldsymbol{v} - D\,\mathbf{grad}\,\tau = 0,\\ &\mathrm{i}\omega\tau + Q\,\mathrm{div}\,\mathbf{grad}\,\tau - R\,\mathrm{div}\,\boldsymbol{v} = 0,\end{aligned} \tag{3}$$

where $B = c^2/\gamma + \mathrm{i}\omega c l_v$, $C = -\mathrm{i}\omega c l'_v$, $D = \mathrm{i}\omega\hat{\beta}/\rho_0$, $Q = -\gamma l_h c$, $R = -(\gamma - 1)/(\gamma\hat{\beta})\rho_0 c^2$, and where the diffusion characteristic lengths are $l'_v = \mu/\rho_0 c$ for shear viscosity, $l_v = (\eta + 4\mu/3)/\rho_0 c$ for bulk viscosity and $l_h = \xi/c$ for thermal diffusion [2].

The use of variables $(\boldsymbol{v}, \tau)$ is relevant, not only to model propagative and diffusive transfers in the bulk of the fluid domain, but also to set the associated physical conditions on the boundaries. The usual boundary conditions are summarized in Table I: non-slip and isothermal conditions on the boundaries are accounted for by Dirichlet conditions; a Neumann condition for τ refers to an adiabatic boundary, and axisymmetrical or symmetry conditions combine Dirichlet and Neumann conditions for temperature variation and particle velocity components.

Models coupling thermoviscous acoustics with the surrounding boundaries can easily be developed in using the same $(\boldsymbol{v}, \tau)$ formulation in the fluid domain [5]:

- thermal diffusion inside the walls can be modeled with the temperature variation formulation, ensuring implicitly the continuity of temperature variation and heat flux by the Finite Element Method,
- when using equation (2) to compute the acoustic pressure trace and accounting for the continuity of the displacement $\boldsymbol{v}/\mathrm{i}\omega$ on the fluid-structure boundary interface, a vibroacoustical model can be developed, using the present $(\boldsymbol{v}, \tau)$ formulation in the thermoviscous fluid and the usual displacement formulation for structural dynamics.

3. Finite element implementation

Under the above assumptions, the coupled equation set (3) accounts for mass, momentum and energy conservation, such that propagative (acoustic waves) and diffusive (heat and momentum transfers) phenomena are described by one vector $\boldsymbol{v}$ and one scalar τ. When a bidimensional mesh is used to represent the fluid domain and to interpolate the field, each node has three degrees of freedom (one for τ and one for each component of $\boldsymbol{v}$). Since these variables are coupled in the bulk of the domain, the numerical computation needs to integrate the equation set locally, as the Finite Element Method does in assembling elementary matrices. Moreover, the Finite Element Method is well suited for this computation because the operators of (3) are similar to the usual mass or stiffness operators (vector operators for $\boldsymbol{v}$ in the first equation, scalar operators for τ in the second one), or first spatial derivative operators for coupling ($\mathbf{grad}\,\tau$ in the first equation and div $\boldsymbol{v}$ in the second one). A matrix form of the equation set (3) is

$$\begin{bmatrix} \omega^2 + \mathbf{div}\,\mathbf{C}\mathsf{grad} & -D\,\mathbf{grad} \\ -R\,\mathbf{div} & \mathrm{i}\omega + Q\,\mathrm{div}\,\mathbf{grad} \end{bmatrix} \begin{Bmatrix} \boldsymbol{v} \\ \tau \end{Bmatrix} = \begin{Bmatrix} \mathbf{0} \\ 0 \end{Bmatrix}, \tag{4}$$

where, similarly to the stiffness tensor of elasticity giving the vector stiffness matrix in the Finite Element modeling of structures, the tensor $\mathbf{C}$ is defined such that $\mathbf{div}\,\mathbf{C}\,\mathsf{grad} = B\,\mathbf{grad}\ \mathrm{div} + C\,\mathbf{curl}\ \mathbf{curl}$ (see Appendix A1). Using Galerkin Finite Elements to integrate the formulation (4), the following linear system is obtained, whose unknown vector is composed of the discrete degrees of freedom for the field $(\boldsymbol{v}, \tau)$,

$$\begin{bmatrix} \omega^2[M_v] + [K_v] & -D[\mathrm{Grad}] \\ -R[\mathrm{Div}] & \mathrm{i}\omega[M_s] + Q[K_s] \end{bmatrix} \begin{Bmatrix} \{\boldsymbol{v}\} \\ \{\tau\} \end{Bmatrix} = \begin{Bmatrix} \mathbf{0} \\ 0 \end{Bmatrix} \tag{5}$$

where (see Appendix A1 and A2 for details)

- the diagonal square matrices are, respectively, the finite element consistent mass- and stiffness-matrices for vector and scalar variables ($[M_v]$ and $[K_v]$ are the consistent mass- and stiffness-matrices of a vector variable, similar to the finite element matrices used to model structural dynamics in a displacement formulation, and $[M_s]$ and $[K_s]$ are the consistent mass- and stiffness-matrices of a scalar variable, similar to the finite element matrices used to model thermal diffusion in a temperature formulation),

- the non-diagonal rectangular matrices [Grad] and [Div] are computed according to their expression occurring in the weak form.
  Note that, due to the above definition of the parameters B and C, the stiffness matrix $[K_v]$ is frequency dependent. In order to benefit from the band structure of the sparse global matrix, it is convenient to reorder the degrees of freedom of the unknown vector in gathering particle velocity and temperature variation variables of a same finite element node.

The Finite Element computation consists of (i) computing the elementary matrices, (ii) assembling the global matrix of (5) which discretizes the local equation set (3) and implicitly accounting for homogeneous boundary conditions of Neumann type, (iii) eliminating the degrees of freedom of Dirichlet boundary conditions. In the case of an homogeneous condition (rigid boundary $\boldsymbol{v} = 0$, isothermal condition $\tau = 0$ or vanishing prescribed condition for some components on a plane of symmetry or in the axisymmetrical axis, see Table I), the corresponding degree of freedom is simply removed; otherwise (exciting velocity of the boundary, prescribed temperature variation) the corresponding prescribed value gives an exciting term that is set in the right hand side of the linear system. A resultant non homogeneous linear set is obtained; then (iv) solving this system of linear equations gives the solution for the degrees of freedom $(\boldsymbol{v}, \tau)$ on the mesh nodes, and finally (v) deriving numerically the velocity vector $\boldsymbol{v}$ according to the mesh interpolation gives the density ρ and acoustic pressure p variations (2).

The particle velocity and temperature variation formulation is then well-suited to a straightforward application of the Galerkin Finite Element Method. Since the coupling between the variables $(\boldsymbol{v}, \tau)$ of the equation set (3) consists of only the first order spatial derivative (terms $\mathbf{grad}\tau$ and $\mathrm{div}\boldsymbol{v}$ of (3), rectangular matrices [Grad] and [Div] in equation 5), the same mesh interpolation is recommended for velocity and temperature variables (the applications presented in section 5 below use isoparametric quadratic triangular elements). As presented in appendix A, the numerical operators used to compute the matrices are the usual interpolation functions or the first order derivation matrices which are commonly used to compute mass and stiffness finite element matrices. When dealing with 'low' frequencies (large time scale relative to molecular relaxation time) and 'large' length scale relative to the mean free path ℓ, we did not encounter the difficulties mentioned in previous communications [20] nor had to use special bubble functions [21] for the elements. The acoustic pressure variation p involves different orders for interpolation (with τ but the first derivative of $\boldsymbol{v}$, equation 2), but the basic computation i.e. the first four steps (i–iv) of the procedure are not concerned by these different orders.

A simple and stable numerical solution of acoustical phenomena in thermoviscous fluids is then obtained by discretizing the particle velocity and temperature variation formulation with the Finite Element Method. However, due to the physics combining very local diffusive processes and propagative phenomena at larger scale, particular attention must be paid to the accuracy of the numerical model. Very accurate solutions are expected for the linear system in complex algebra (step iv), but the computational cost and the accuracy of the result are first determined by the quality of the mesh. The physics and its practical consequences on the numerical computation are discussed in next section.

4. Adaptive meshing procedure

To model numerically some phenomena, a suitable formulation and an efficient numerical method are obviously needed, but the order of magnitude of the different physical processes and scale effects also need to be considered. The $(\boldsymbol{v}, \tau)$ formulation and the Finite Element Method presented in the previous sections take the first two of these conditions into account, and special care has to be taken in designing the mesh to meet the third one. As illustrated in Figure 1, the smallest length scale for the field is determined by the boundary layer thicknesses (δ_h, δ_v). The temperature and velocity fields spatially oscillates inside the boundary layer thicknesses, such that the required distance between the finite element nodes has often to be much smaller than (δ_h, δ_v). Considering this smallest scale to mesh the whole acoustic volume would lead to an enormous number of degrees of freedom, and to an unreasonable computational cost for the numerical solution. Strong variations of the field at such very small length scale are physically confined inside the boundary layers, or at least not too far from the boundaries. In contrast, in the bulk of the domain, the field is structured with another characteristic length, the acoustic wavelength λ, which is larger by several order of magnitude $\lambda \gg (\delta_h, \delta_v)$ (see Figure 1). Both scales (δ_h, δ_v) and λ are larger at low frequencies, allowing the use of elements of larger size but, due to different slope in Figure 1 for the characteristic lengths (1) versus frequency, the magnitude of the difference is still larger. To avoid very numerous nodes for the mesh, the size of the finite elements then can be adjusted to the wavelength in the fluid volume, but proportionately refined when moving near the boundaries. This method is convenient to generate a suitable mesh set, allowing the adequate interpolation at the wavelength scale for acoustic propagation in the fluid volume, and at diffusion length scales inside the boundary layers and near the boundaries. Since normal and tangential second derivatives of the field differ by orders of magnitude inside the boundary layers, an anisotropic distribution of the finite element nodes is required, and the optimal mesh is then anisotropic. The criterion for mesh adapting is then based on the Hessian matrix, composed of the second derivative of a degree of freedom; adaptive meshing built from the Laplacian of the field, giving isotropic meshes, is not suited to model efficiently the boundary layers.

Building the appropriate anisotropic mesh for a given configuration is a nontrivial task, because the right size for the elements is not precisely known out of hand, and

because some recirculating flow or vortices may occur, especially near angular points or high curvature boundaries, which require refined meshes at distances much larger than the thickness of plane boundary layers. To obtain the right mesh, a reliable method is to update the mesh according to the physical solution for the field, in adapting iteratively the anisotropic mesh to minimize the interpolation error. Such an adaptive meshing procedure is available [27]. Starting with a first metric corresponding to an isotropic and very coarse mesh, it consists in

1. building the mesh, according to the metric,
2. computing the Finite Element solution of the physics, on this mesh (steps (i) to (iv) of the procedure detailed in section 3),
3. computing the Hessian matrix (2nd order derivative) of the complex modulus of the solution for variables $\boldsymbol{v}$ and τ, according to the interpolation on the mesh,
4. computing the anisotropic metric minimizing the interpolation error (the local size and the orientation of the elements are defined such that the interpolation error is equally distributed on the surface of the mesh),
5. building the global metric in intersecting the metrics for $\boldsymbol{v}$ and τ (in keeping the smallest size for the element),
6. going back to step 1),

until convergence.

When compared to a manually made definition of the parameters for the mesh, this procedure is considerably easier for the modeling end-user to obtain a reliable mesh. The adaptive meshing procedure is very efficient to optimize the anisotropic mesh for multiphysics and multiscale problems. In the case of thermoviscous acoustics, it allows to increase the node density in the right place and in accordance with the orientation and the anisotropy of the physical field, and converges to an optimal mesh. When beginning with a coarse mesh, the starting loops of the procedure are very fast computed because the first meshes have only very few nodes. The mesh is thereafter refined, especially in the normal direction near the boundaries, and therefore the number of nodes and the computation time increase. According to the physics, the metric is bounded such that the distance between mesh nodes is far greater than the mean free path ℓ in the fluid and, as usual in computing numerically acoustic fields, smaller than one sixth of the acoustic wavelength λ (1).

In the application examples presented below, except for the finite element computation (step 2), the steps 1–6 of the adaptive mesh procedure are computed with the Bidimensional Anisotropic Mesh Generator [27]; this code was experienced to converge stable and robust solutions for acoustics in thermoviscous fluids. The graphics have been obtained on the basis of the code GRAME [28].

5. Applications

The numerical procedure presented above can be used to compute accurate acoustic field for the models applied to acoustical calibration, device development (acoustical transducers, MEMS, thermoacoustics, microfluidics), analysis of complex or porous materials, or to validate assumptions used in other analytical models. Two examples are presented in order to show the potential of such computations and how precise and detailed physical processes can be analyzed and illustrated.

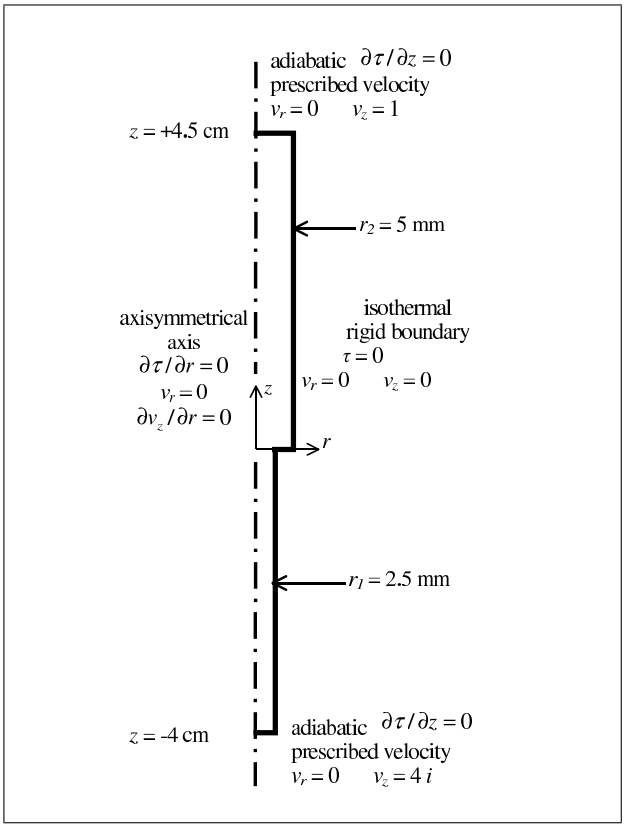


Figure 2. Axisymmetrical model of a cylindrical duct with a sudden doubling radius.

The formulation and the numerical techniques presented above are suited for both bi-dimensional or three-dimensional models, regardless of the coordinate system used (Cartesian, cylindrical or spherical). The computation of thermoviscous acoustic fields is easily performed on bi-dimensional meshes for (x, y) planar (invariant field along the third direction of space) or (r, z) axisymmetrical models. The latter solution is suited to study cylindrical devices like microphones [29]. Another application is presented below (section 5.1) to model the local field for a propagative wave in a straight duct near a sudden doubling radius. A bidimensional model is presented in section 5.2, applying the method to compute the standing wave field in a closed rectangular cavity where a stack of seven plates has been inserted.

5.1. Axisymmetrical model: propagative wave in a duct at a sudden doubling radius

An axisymmetrical straight duct is considered, of vertical axis z, filled by air ($c = 340\,\mathrm{m/s}$, $\rho_0 = 1.2\,\mathrm{kg/m^{-3}}$), where the lower part ($z < 0$) of the tube is $r_1 = 2.5\,\mathrm{mm}$ in radius. The radius is doubled ($r_2 = 5\,\mathrm{mm}$) in the upper part, expanding the cross section by a factor four (Figure 2). A

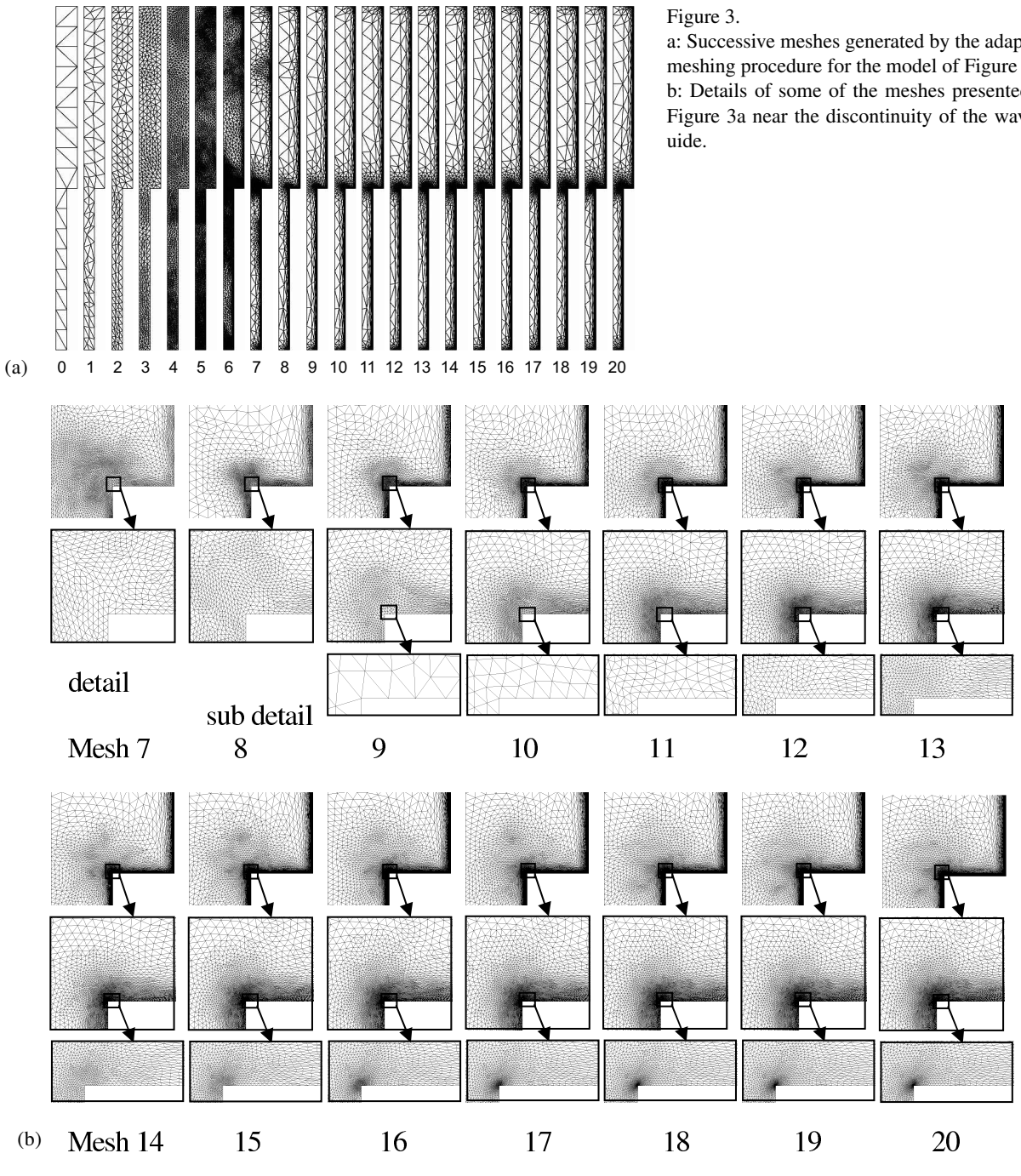


Figure 3.
a: Successive meshes generated by the adaptive meshing procedure for the model of Figure 2.
b: Details of some of the meshes presented in Figure 3a near the discontinuity of the waveguide.

1 kHz propagative wave is considered in the $+z$ direction. The domain meshed for the axisymmetrical computation is one half section of the device. The boundary conditions are (Figure 2):

- axisymmetrical conditions (see Table I) on the left axis,
- isothermal (thermal) and rigid (mechanical) conditions in the walls of the duct and the discontinuity ($z = 0$, $r_1 < r < r_2$),
- in order to approximate a propagative wave directed upward, the bottom ($z = -4$ cm) and top ($z = +4.5$ cm) end cross sections are adiabatic and plane pistons ($v_r = 0$, prescribed v_z). Since the total high of the duct model is approximately one quarter of a wavelength, the imposed velocity of both ends is shifted of $\pi/2$ in phase and have a modulus proportional to the inverse of the cross section, to develop a conservative acoustical fluid flow for the propagative wave.

The convergence of the adaptive meshing procedure (section 4) is illustrated on Figures 3a,b. The very coarse initial mesh (0) is first refined uniformly (meshes 1–6). After these iterations, when the accuracy of the computation is enough to figure the boundary layers, the mesh is refined and anisotropic inside the boundary layers, and approximately isotropic and enlarged when far from the bound-

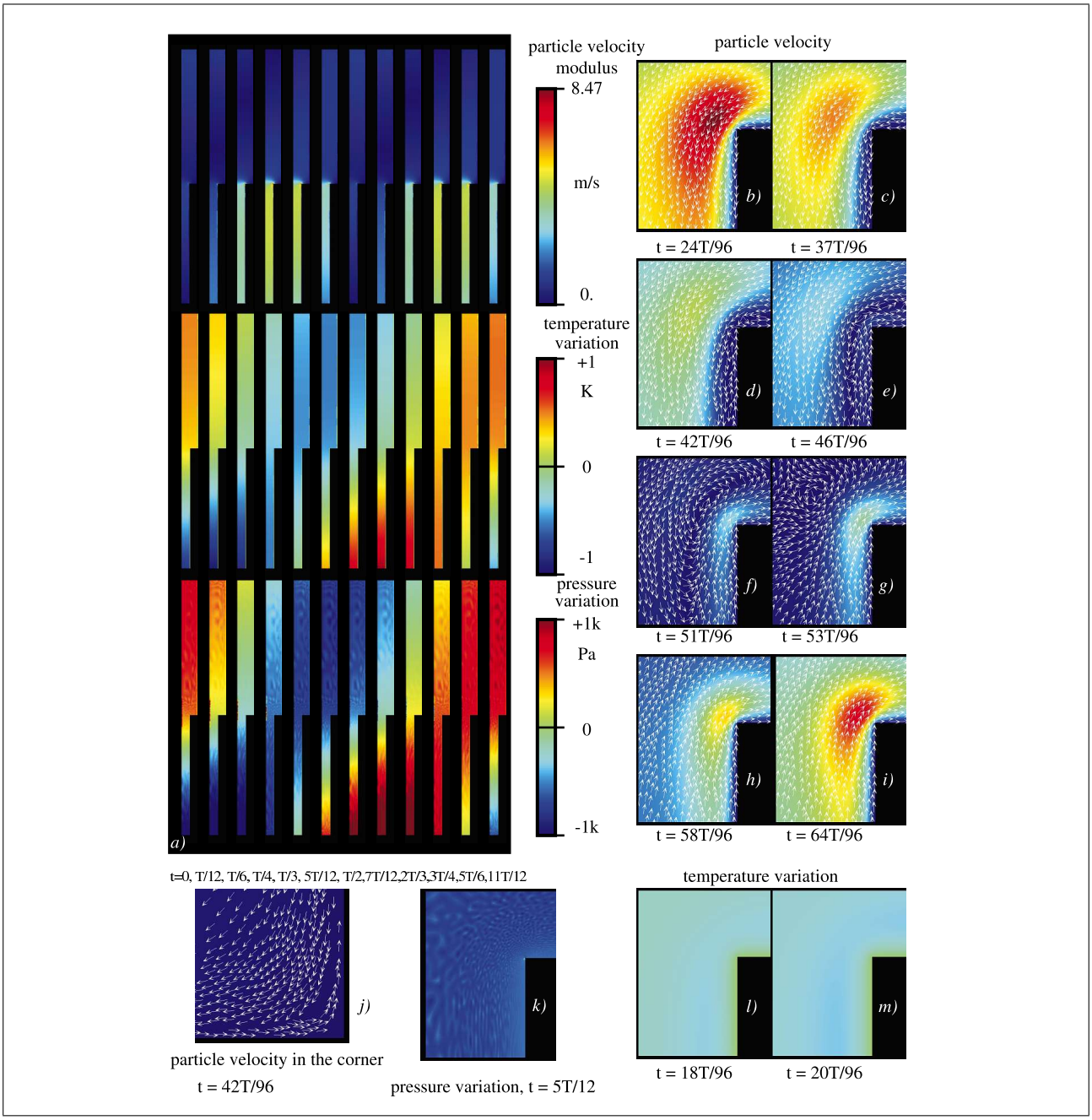


Figure 4. Particle velocity (colormap = modulus, arrows = orientation), temperature and pressure variations in the device of Figure 2: evolution of the field during the harmonic period (a), detail of the particle velocity field near the discontinuity (b–i) and in the corner (j) of the waveguide, detail of the pressure variation (k) and of the temperature variation (l,m) near the discontinuity.

aries (meshes 7–8), such that the interpolation error of the physical field is equally distributed in the mesh. The anisotropic mesh is then progressively refined inside the boundary layers and near the discontinuity ($z = 0$) of the duct (meshes 8–20), to focus the computational effort exactly where the variation of variables ($\boldsymbol{v}, \tau$) is more intensive. Because of the very small length scales inside the boundary layers, the last improvement of the mesh is not clearly visible on Figure 3a, but the details presented in Figure 3b near the discontinuity of the waveguide ($z = 0$, $r = r_1$) illustrate the progressive refinement of the mesh near the discontinuity of the duct.

The result of the computation on the mesh number 20 is presented in Figure 4, where the upward propagative character of the wave is illustrated in Figure 3a for the particle velocity $\boldsymbol{v}$, the temperature variation τ and the pressure variation p at different time t of the harmonic period T. The particle velocity (Figure 4a, up) is more intensive in the lower part ($z < 0$) of the duct, due to the smaller cross section. In the center of the device, the particle velocity is oriented downward during the first part of the period, and upward in the second one. The smallest values for the velocity occurs at $t = 0$ and $t = T/2$ on the bottom section, and propagates upward according to the sound ve-

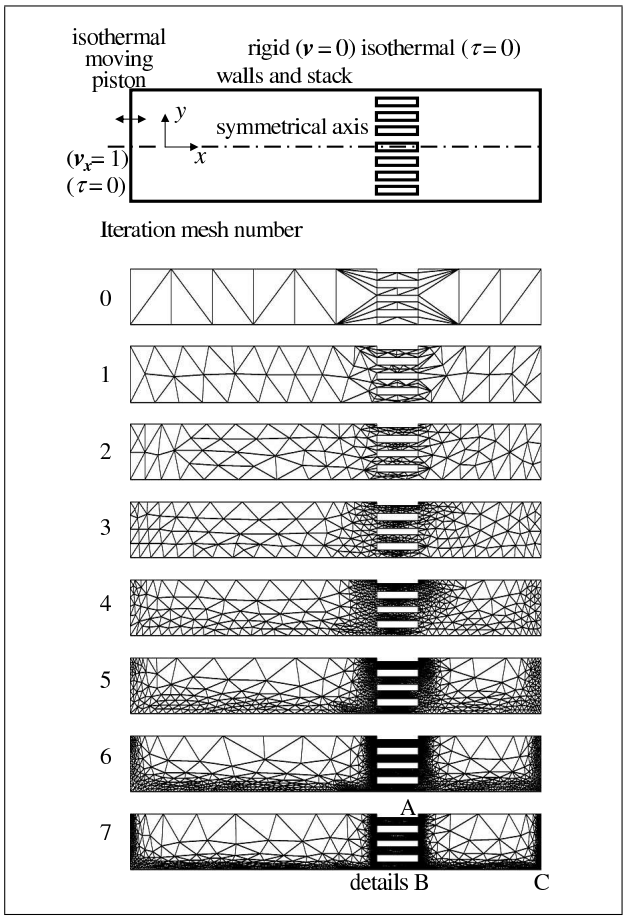


Figure 5. Bidimensional model in the plane (x, y) and successive meshes of a resonant cavity including a stack. Letters A,B,C in the bottom mesh localize the detailed field of Figure 6.

locity. The vanishing zones and extrema for temperature and pressure variations can be tracked during the period T on Figure 4a, showing the propagative wave in the duct. Detailed views of the particle velocity modulus and orientation are presented near the discontinuity on Figures 4b–i. A very intensive velocity occurs when the velocity anti-node crosses the discontinuity $z = 0$ at $t = T/4$ (Figure 4b): the local maximum amplitude (8.47 m/s) is more than twice the maximum velocity amplitude of the wave in the lower part of the tube ($z < 0$, 4 m/s), giving very high velocity gradients and intensive shear movement of the fluid to satisfy the non slip condition $\boldsymbol{v} = 0$ on the wall. The flow then decreases in time (Figure 4c) and, due to small velocity and small inertial effect, a very weak counter-flow occurs just near the wall ($t = 42T/96$, Figure 4d). In accordance with the diffusive character of shear waves, the momentum diffuses from the boundary to the bulk of the fluid, growing the section of the inverted flow (Figure 4d,e). The line of vanishing velocity ($\boldsymbol{v} = 0$, deep blue in Figures 4d,e,f) leaves the neighbor of the discontinuity (Figure 4e,f,g), a transient vortex develops and moves away (Figure 4f,g) and the inverted flow becomes more intensive near the discontinuity (Figure 4g,h,i) until the next passing of a velocity anti-node. Another half period then starts at $t = 3T/4$ with exactly the same progress and the same amplitude but opposite direction for the flow. Figures 4b–j illustrate the diffusive process for momentum, born on the boundary and transferred in the viscous boundary layer to the bulk of the fluid. Thermal diffusion develops in a very similar process, as illustrated in Figures 4l,m: due to the isothermal condition $\tau = 0$ on the boundary, the temperature variation vanishes when approaching the boundary, even when the temperature variation is pretty strong in the bulk of the fluid. To satisfy this isothermal boundary condition, the thermal perturbation caused by transfers with the boundaries starts on the boundary, and is then diffused into the fluid domain. When combined with the temperature variation caused by the acoustical movement, this thermal boundary effect produces an extremum for the total temperature variation, diffusing from the boundary: the deep blue line has moved away from the boundary from $t = 18T/96$ to $t = 20T/96$ on Figures 4l,m. In contrast, no boundary layer effect can be observed for pressure variation: even for the pressure anti-node, the pressure field is very homogeneous near the discontinuity (see detail near the discontinuity on Figure 4k).

Since convective and other non-linear effects are neglected, the harmonic solution of the linearized equations shows the same progress but opposite temperature variation and particle velocity orientation during the first and the second half period ($0 < t < T/2$, $T/2 < t < T$). Such an anti-symmetry cannot develop different vortices during ejection and suction phases. This structure for the flow matches with experimental particle image velocimetry analysis of the acoustic flow at low acoustic levels [30].

5.2. Bidimensional model: resonance of a cavity including a stack

The second application concerns a closed cavity of dimension 100 mm long, 15 mm high and infinite in the third direction, excited by a plane piston at the left end. A stack composed of seven plates, 10 mm long, is centered at 65 mm from the piston. The air gap between the plates and their thickness is 1 mm. The harmonic motion of the piston is 1 m/s in amplitude at 1.7 kHz, such that the length of the cavity would be half of a wavelength for a plane acoustic wave propagating in free field. The system is invariant in one direction and symmetric, and only one half of the bidimensional fluid domain is meshed. The upper face of the mesh is the symmetrical axis $y = 0$ (adiabatic $\partial\tau/\partial y = 0$, $\partial v_x/\partial y = 0$, $v_y = 0$), the walls and the boundaries of the stack are rigid ($\boldsymbol{v} = 0$) and isothermal ($\tau = 0$); the horizontal motion of the left piston is harmonic ($v_x = 1$, $v_y = 0$) and isothermal (Figure 5). The device is not symmetric in the axis direction because of the presence of the stack and because of different velocity conditions on the left and right ends.

The first iterations for the mesh adapting procedure are illustrated on Figure 5: a very coarse mesh is initialized (0), and the procedure refines the mesh in the boundary layers, on the boundaries and near or inside the stack

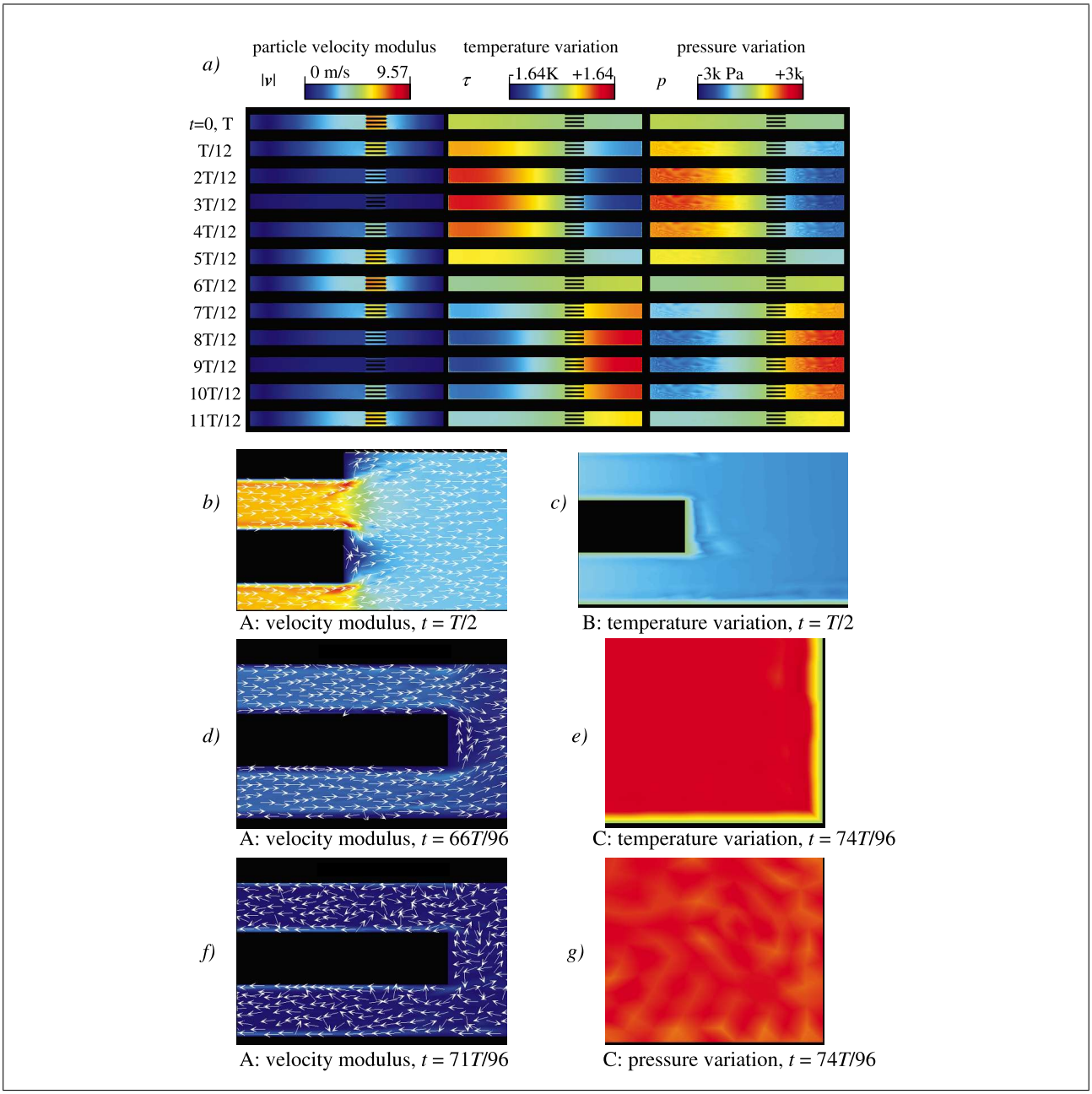


Figure 6. Particle velocity (colormap = modulus, arrows = orientation), temperature and pressure variations in the device of Figure 5: evolution of the field during the harmonic period (a), detail of the field at time $t = T/2$ (b,c), $t = 66T/96$ (d), $t = 71T/96$ (f), $t = 74T/96$ (e,g).

(meshes 1–7). Far from the boundaries, the acoustic field is very smooth and large elements are used, in particular near the symmetry plane. Figure 6a illustrates the acoustic resonance inside the cavity. The velocity modulus, temperature and pressure variations are presented at each 1/12 of the period T: the particle velocity is more intensive at time $t = 0$ and $t = T/2$, in phase with the motion of the piston, while extrema of temperature and pressure variations occur at $t = T/4$ and $t = 3T/4$. The pressure field is very smooth, even just near the boundaries and in the stack (see Figure 6g), but as mentioned above and due to numerical differentiate, its computation is sensitive to interpolation errors. Detailed views of the flow around the end of the stack are presented in Figures 6b,d,f: the intensive flow at $t = 0$, $t = T/2$ (Figure 6b) develops high velocity gradients and shear effects at the end of the plate, without significant rollup, according to the linear theory and experimental particle image velocimetry measurements [31] at low acoustic level when the plate thickness (1 mm) is similar to the viscous boundary layer thickness δ_ν (see Figure 1 at 1 kHz). As observed in section 5.1 inside the boundary layers effects during the period T, the flow inverts first just near the rigid boundaries (Figure 6d) and then diffuses in the section of the fluid. As expected, thermal boundary layers develop near the isothermal boundaries (Figure 6c,e).

6. Conclusion

The numerical computation of thermoviscous acoustics consists of multi-physics and multi-scale modeling, combining propagative or resonant acoustic processes characterized by the wavelength, and diffusive processes for momentum and heat transfers in boundary layers of much smaller thicknesses. When using anisotropic meshes and a convenient adaptive procedure, harmonic solution is obtained for this problem with the finite element method and a particle velocity and temperature variation formulation at reasonable computational cost: for instance, the full computation for iterative meshing and solving for the results of section 5.2 (Figures 5–6) is 30 minutes with one CPU Intel Xeon 2.33 GHz, where the matrix (5) building takes less than 5 seconds in the last iteration (36327 degrees of freedom). Taking advantage of the complex notation for harmonic solutions and because the computational effort is focused exactly where needed by the physical field in using adaptive meshing, complete devices of complicated geometry can be efficiently modeled, when the cost of other computational approaches often lead to consider only subsystems. The examples of application presented in section 5 show that the numerical computation using the assumptions of a small acoustic perturbation and linear approximation reasonably models the physics of both acoustics (propagation, resonances) and boundary layers (thermal and viscous).

The formulation and the matrices (Appendix A1) can be used for three-dimensional models, provided an adaptive meshing procedure is used for volume meshes. When accounting for the continuity of velocity and of the trace of pressure variation and viscous stress on the interface with the surrounding structure, this formulation can be extended to vibro-acoustic models for thermoviscous fluids. Another possible extension is the modeling in the time domain: the basic formulation based upon particle velocity and temperature variation can be used in the time domain [5], in starting from initial conditions the time integration. However, the mesh adapting procedure should be performed until convergence at each time step, the smallest length scale of the mesh being prescribed by the highest frequency in the acoustic signal. When dealing with harmonic solutions, the Finite Element Method using degrees of freedom for acoustical particle velocity and temperature variation combined with adaptive anisotropic meshing technique is well-suited to model precise acoustic field in thermoviscous fluids.

Appendix A1: Galerkin Finite Elements for bidimensional models

In the following developments, some notations are used,

- the fluid domain Ω has a boundary Γ,
- the gradient of a vector $\boldsymbol{v}$ and the divergence of a tensor $\mathbf{T}$ are defined as

$$\left(\mathrm{grad}\,\boldsymbol{v}\right)_{ij} = \frac{\partial v_i}{\partial x_j}, \quad \left(\mathrm{div}\,\mathbf{T}\right)_i = \frac{\partial T_{ij}}{\partial x_j},$$

  where implicit summation is used for repeated indices,

- the tensor $\mathbf{C}$ of equation (4) is defined as

$$c_{ijkl} = (2A + B)\delta_{ij}\delta_{kl} - A(\delta_{ik}\delta_{jl} + \delta_{il}\delta_{jk}), \tag{A1}$$

  where δ_{ij} is the Kronecker symbol ($\delta_{ii} = 1$ and $\delta_{i\neq j} = 0$), such that $\mathbf{C}\,\mathrm{grad}\,\boldsymbol{v}$ is a symmetric tensor whose divergence is $\mathbf{div}\,\mathbf{C}\,\mathrm{grad}\,\boldsymbol{v} = B\,\mathbf{grad}\,\mathrm{div}\,\boldsymbol{v} + A\,\mathbf{curl\,curl}\,\boldsymbol{v}$,
- ${}^t[A]$ is the notation for the transposed matrix $[A]$.

Local interpolation of scalar and vector fields and their first derivatives on isoparametric bidimensional elements

We consider a bidimensional Finite Element e with local parameters (ξ, η), of n nodes, and we use the subscript α to denote the nodes of the elements, $\alpha = 1$ to n, with implicit summation on α when this subscript is presented twice. The coordinate of the nodes are (x_α, y_α) in a bidimensional space (x, y). On this element e, a variable σ is interpolated as

$$\sigma_e = \left\langle N_\alpha \right\rangle \left\{\sigma_\alpha\right\}, \tag{A2}$$

where $N_\alpha(\xi, \eta)$ are the interpolation functions associated to each node, in a row vector, and σ_α are the values of σ on each node, i.e. the degrees of freedom on the mesh, in a column vector. For an isoparametric element, the geometry is interpolated according to (A.2) $x_e = \langle N_\alpha\rangle\{x_\alpha\}$, $y_e = \langle N_\alpha\rangle\{y_\alpha\}$, such that the Jacobian matrix expresses as

$$\left[J\right] = \begin{bmatrix} \partial x/\partial\xi & \partial x/\partial\xi \\ \partial x/\partial\eta & \partial y/\partial\eta \end{bmatrix} = \begin{bmatrix} \partial N_\alpha/\partial\xi \\ \partial N_\alpha/\partial\eta \end{bmatrix} \begin{bmatrix} x_\alpha & y_\alpha \end{bmatrix},$$

where $\left[\partial N_\alpha/\partial\xi \;\; \partial N_\alpha/\partial\eta\right]$ is the matrix of the local derivatives of the interpolation functions and $\left[x_\alpha \; y_\alpha\right]$ the matrix of the nodes coordinates of the element. The gradient of variable σ is therefore interpolated as

$$\begin{aligned} \mathbf{grad}\,\sigma_e &= \left[J\right]^{-1} \begin{bmatrix} \partial N_\alpha/\partial\xi \\ \partial N_\alpha/\partial\eta \end{bmatrix} \left\{\sigma_\alpha\right\} \\ &= [\mathrm{grad}]\{\sigma_\alpha\}. \end{aligned} \tag{A3}$$

When considering a vector variable like the particle velocity $\boldsymbol{v}$, each of its components (v_x, v_y) is interpolated according to (A.2) in using, respectively, the degrees of freedom of the x or y component of the particle velocity on the element $\boldsymbol{v}_{xe} = \langle N_\alpha\rangle\{\boldsymbol{v}_{x\alpha}\}$, $\boldsymbol{v}_{ye} = \langle N_\alpha\rangle\{\boldsymbol{v}_{y\alpha}\}$. Combining these components for a single vector $\boldsymbol{v}_\alpha = \left\{v_{x\alpha} \; v_{y\alpha}\right\}$, the velocity is interpolated on the element e as

$$\boldsymbol{v}_e = \left[N_\alpha\right]\left\{\boldsymbol{v}_\alpha\right\}, \tag{A4}$$

where one row of the matrix $[N_\alpha]$ is composed of the interpolation function $N_\alpha(\xi, \eta)$ for the columns of the degrees of freedom of the corresponding component (x or y), completed by zeros for the other (y or x). Similarly, according to (A3), the vector gradient of one component x or y of the velocity vector expresses as $\mathbf{grad}\,\boldsymbol{v}_{xe} = [\mathrm{grad}]\{\boldsymbol{v}_{x\alpha}\}$

or $\mathbf{grad}\, \boldsymbol{v}_{ye} = [\mathrm{grad}]\{\boldsymbol{v}_{y\alpha}\}$, that may be condensed in the form

$$\begin{Bmatrix} \partial \boldsymbol{v}_x/\partial x \\ \partial \boldsymbol{v}_y/\partial y \\ \partial \boldsymbol{v}_y/\partial x \\ \partial \boldsymbol{v}_x/\partial y \end{Bmatrix} = \big[\mathbf{grad}\big]\big\{\boldsymbol{v}_\alpha\big\}, \tag{A5}$$

where the components of the tensor $\mathbf{grad}\boldsymbol{v}$ are stored in the vector $\mathbf{grad}\, \boldsymbol{v}_e = \big\{\partial \boldsymbol{v}_x/\partial x\ \partial \boldsymbol{v}_y/\partial y\ \partial \boldsymbol{v}_y/\partial x\ \partial \boldsymbol{v}_x/\partial y\big\}$. The particle velocity divergence is obtained by the summation of the two first components, and may be expressed as

$$\mathrm{div}\, \boldsymbol{v}_e = \big\langle \mathrm{div}\big\rangle\big\{\boldsymbol{v}_\alpha\big\}, \tag{A6}$$

where the row vector $\langle \mathrm{div}\rangle$ for interpolation of the divergence is the summation of the two first lines of the matrix [**grad**]. Relation (A.6) is used to interpolate the particle velocity divergence for the post-processing computation of the pressure variation (2).

The relations (A.2-6) may be summarized as follows for the local interpolation of the field $(\boldsymbol{v}, \tau)$ and its first derivatives, where the subscript α for the nodes is omitted,

$$\begin{aligned} &\tau_e = \langle N\rangle\{\tau\}, && \boldsymbol{v}_e = [N]\{\boldsymbol{v}\}, \\ &\mathbf{grad}\, \tau_e = [\mathrm{grad}]\,\{\tau\}, && \mathbf{grad}\, \boldsymbol{v}_e = [\mathbf{grad}]\,\{\boldsymbol{v}\}, \\ & && \mathrm{div}\, \boldsymbol{v}_e = \langle \mathrm{div}\rangle\{\boldsymbol{v}\}. \end{aligned} \tag{A7}$$

Note that (i) due to the Jacobian matrix for the computation of the gradient (A.3), the interpolation matrices [grad] and [**grad**] and interpolation row $\langle \mathrm{div}\rangle$ depend on the element geometry, (ii) the vectors $\{\tau\}$ and $\{\boldsymbol{v}\}$ used for this interpolations are the local degrees of freedom of the current element e, and the interpolation rows $\langle N\rangle$, $\langle \mathrm{div}\rangle$ or matrices $[N]$, [grad], [**grad**] are local interpolation functions, which differ from the global assembled matrices presented in section 3.

Galerkin Finite Element and matrices of equation set (5)

The weak formulation of the coupled problem (3) is obtained in taking the dot product of the first equation by a vector test-function $\boldsymbol{w}$, the product of the second one by a scalar test function w, and therefore integrating by part on the fluid domain Ω. Denoting $\boldsymbol{n}$ the external normal vector, it writes

$$\begin{aligned} &\omega^2 \int_\Omega \boldsymbol{w}\cdot\boldsymbol{v}\,\mathrm{d}\Omega - \int_\Omega {}^t(\mathbf{grad}\, \boldsymbol{w}) : \mathbf{C}\,\mathbf{grad}\, \boldsymbol{v}\,\mathrm{d}\Omega \\ &-D\int_\Omega \boldsymbol{w}\cdot\mathbf{grad}\,\tau\,\mathrm{d}\Omega + \int_\Gamma \big((\mathbf{C}\,\mathbf{grad}\,\mathrm{v})\boldsymbol{n}\big)\cdot\boldsymbol{w}\,\mathrm{d}\Gamma = 0, \\ &\mathrm{i}\omega\int_\Omega w\tau\,\mathrm{d}\Omega - Q\int_\Omega \mathbf{grad}\, w\cdot\mathbf{grad}\,\tau\,\mathrm{d}\Omega \\ &-R\int_\Omega w\,\mathrm{div}\, v\,\mathrm{d}\Omega + Q\int_\Gamma w(\mathbf{grad}\,\tau\cdot\boldsymbol{n})\,\mathrm{d}\Gamma = 0, \end{aligned}$$

where the boundary integrals $\int_\Gamma \ldots \mathrm{d}\Gamma$ vanish, either due to homogeneous Neumann boundary condition or to vanishing test function for Dirichlet condition on the boundary Γ (see Table I). When interpolating the field $(\boldsymbol{v}, \tau)$ by relations (A.7) and the test functions $(\boldsymbol{w}, w)$ in a similar way,

$$\begin{aligned} &w_e = \langle N\rangle\{w\}, && \boldsymbol{w}_e = [N]\{\boldsymbol{w}\}, \\ &\mathbf{grad}\, w_e = [\mathrm{grad}]\,\{w\}, && \mathbf{grad}\, \boldsymbol{w}_e = [\mathbf{grad}]\,\{\boldsymbol{w}\}, \end{aligned}$$

and expressing the integral on the domain Ω as the summation of the integrals on each of the elements e of the mesh $\int_\Omega \ldots \mathrm{d}\Omega = \sum_{e\in\mathrm{Mesh}} \int_e \ldots \mathrm{d}x\,\mathrm{d}y$, the integrals of the above weak formulation are written from the following local matrices. The summation over all the elements of the mesh gives the global assembled matrices

Local matrices	Assembled matrices
Consistent vector mass matrices:	
$[m_v] = \int_e {}^t[N][N]\,\mathrm{d}x\,\mathrm{d}y$	$[M_v]$
Vector stiffness matrices:	
$[k_v] = \int_e {}^t[\mathbf{grad}][C][\mathbf{grad}]\,\mathrm{d}x\,\mathrm{d}y$	$[K_v]$
Temperature gradient coupling matrices:	
$[c_{\tau v}] = \int_e {}^t[N][\mathrm{grad}]\,\mathrm{d}x\,\mathrm{d}y$	[Grad]
Consistent scalar mass matrices:	
$[m_s] = \int_e {}^t\langle N\rangle\langle N\rangle\,\mathrm{d}x\,\mathrm{d}y$	$[M_s]$
Scalar stiffness matrices:	
$[k_s] = \int_e {}^t[\mathrm{grad}][\mathrm{grad}]\,\mathrm{d}x\,\mathrm{d}y$	$[K_s]$
Velocity divergence coupling matrices:	
$[c_{v\tau}] = \int_e {}^t\langle N\rangle\langle \mathrm{div}\rangle\,\mathrm{d}x\,\mathrm{d}y$	[Div]

where, for the computation of $[k_v]$, the symmetric matrix $[C]$ contains the coefficients (A.1). Local matrices are full. The assembled consistent mass and stiffness matrices are square, symmetric and sparse band matrices; rectangular matrices [Grad] and [Div] are sparse band, but cause the non-symmetry of the global system. Renumbering the nodes of the mesh and reordering together the degrees of freedom $(\boldsymbol{v}, \tau)$ of a same node in the linear system (5) reduces the band size of the global matrix, giving a nonsymmetric complex sparse band linear equation set.

Appendix A2: Galerkin Finite Elements for axisymmetrical models

The meshes used in axisymmetrical models are planar, in one half section of the fluid domain, where one element represents the volume generated in revolving its surface around the axissymmetrical axis z. The space coordinate of axisymmetrical models is (r, z), where r denotes the radius. The differential operators in axisymmetrical coordinates (r, z) are similar to operators in bidimensional Cartesian space (x, y) where r corresponds to x and z to y, except for divergence operators and the gradient of a vector (in cylindrical coordinates (r, θ, z), where θ is the azimuthal direction)

$$\begin{aligned} \mathbf{grad}\, \boldsymbol{v} &= \begin{bmatrix} \partial v_r/\partial r & 0 & \partial v_r/\partial z \\ 0 & v_r/r & 0 \\ \partial v_z/\partial r & 0 & \partial v_z/\partial z \end{bmatrix}, \\ \mathbf{div}\, \mathbf{T} &= \begin{Bmatrix} \partial T_{rr}/\partial r + \partial T_{rz}/\partial z + T_{rr}/r \\ 0 \\ \partial T_{zr}/\partial r + \partial T_{zz}/\partial z + T_{zr}/r \end{Bmatrix}, \\ \mathrm{div}\, \boldsymbol{v} &= \mathrm{tr}\big(\mathbf{grad}\, \boldsymbol{v}\big) = \frac{\partial v_r}{\partial r} + \frac{\partial v_z}{\partial z} + \frac{v_r}{r}, \end{aligned} \tag{A8}$$

where tr(...) denotes the trace.

Expressions for local matrices $[m_v]$, $[c_{\tau v}]$, $[m_s]$ and $[k_s]$ are then the same as those of the Appendix A1 in bidimensional space, where axisymmetrical integrals $\int_e \ldots 2\pi r \, \mathrm{d}r \, \mathrm{d}z$ are substituted to the integrals $\int_e \ldots \mathrm{d}x \, \mathrm{d}y$. The same change of variables is used for integration of matrices $[c_{vr}]$ and $[k_v]$, where in addition the term $\boldsymbol{v}_r/r$ occurring in (A8) for **grad** $\boldsymbol{v}$ and (div $\boldsymbol{v}$) must be accounted for. In the case of the vector stiffness matrix $[k_v]$, the term $\boldsymbol{v}_r/r$ in **grad** $\boldsymbol{v}$ is oriented in the azimuthal direction θ, such that the symmetric matrix $[C]$ for parameters (A1) must be defined for the three directions of space.

Acknowledgement

The author gratefully acknowledge F. Hecht for the mesh adapting procedure software BAMG [27], P. Gentil for the graphic routine GRAME [28], and M. Bruneau and O. Dazel for valuable discussions in the Laboratoire d'Acoustique de l'Université du Maine.

References

[1] G. Kirchhoff: Über den Einfluss der Wärmeleitung in einem Gase auf die Schallbewegung. Annalen der Physik, Leipzig, 1868. (English translation in R.B. Lindsay, Physical acoustics, Dowden, Hutchinson and Ross, Stroudsburg, 1974).

[2] M. Bruneau, T. Scelo: Fundamentals of acoustics. ISTE, 2006.

[3] L. Cremer: On the acoustic boundary layer outside a rigid wall. Arch. Elektr. Uebertr. **2** (1948) 235.

[4] R. Bossart, N. Joly, M. Bruneau: Hybrid numerical and analytical solutions for acoustic boundary problems in thermoviscous fluids. J. Sound Vib. **263** (2003) 69–84.

[5] N. Joly, M. Bruneau, R. Bossart: Coupled equations for particle velocity and temperature variation as the fundamental formulation of linear acoustics in thermo-viscous fluids at rest. Acta Acustica united with Acustica **92** (2006) 202–209.

[6] A. Cummings: Sound propagation in narrow tubes of arbitrary cross-section. J. Sound Vib. **162** (1993) 27–42.

[7] M. Bruneau, P. Herzog, J. Kergomard, J. D. Polak: General formulation of the dispersion equation in bounded viscothermal fluid, and application to some simple geometries. Wave Motion **11** (1989) 441–451.

[8] M. Bruneau, A.-M. Bruneau, Z. Skvor, P. Lotton: An electrical network to modelling the strong coupling between a vibrating membrane and a fluid film. Acta Acustica **2** (1994) 223–232.

[9] M. Bruneau, A.-M. Bruneau, P. Dupire: A model for rectangular miniaturized microphones. Acta Acustica **3** (1995) 275–282.

[10] T. Le Van Suu, S. Durand, M. Bruneau: Fluid layer trapped between a plane, circular membrane and axisymmetrically curved, smooth backing wall: analytical model of the dynamic behaviour. Acta Acustica united with Acustica **94** (2008) 474–482.

[11] M. Moser: Damping of structure born sound by the viscosity of a layer between two plates. Acustica **46** (1980) 210–217.

[12] T. Veijola, A. Lehtovuori: Numerical and analytical modeling of trapped gas in micromechanical squeeze-film dampers. J. Sound Vib. **319** (2009) 606–621.

[13] M. Moldover, J. Mehl, M. Greenspan: Gas-filled spherical resonators: Theory and experiment. J. Acoust. Soc. Am. **79** (1986) 253–271.

[14] C. Guianvarc'h, J.-N. Durocher, M. Bruneau, A.-M. Bruneau: Acoustic transfer admittance of cylindrical cavities. J. Sound Vib. **292** (2006) 595–603.

[15] C. Karra, M. Ben Tahar: Modélisation par éléments finis de frontières du comportement vibratoire d'une membrane couplée à une couche de fluide thermoconducteur. C. R. Acad. Sci. Paris 326 II b (1998) 733–739.

[16] C. Karra, M. Ben Tahar: An integral equation formulation for boundary element analysis of propagation in viscothermal fluids. J. Acoust. Soc. Am. **102** (1997) 1311–1318.

[17] E. Dokumaci: An integral equation formulation for boundary element analysis of acoustic radiation problems in viscous fluids. J. Sound Vib. **147** (1991) 335–348.

[18] W. M. Beltman, P. J. M. Van der Hoogt, R. M. E. Spiering, H. Tijdeman: Implementation and experimental validation of a new viscothermal acoustic finite element for acousto-elastic problems. J. Sound Vib. **216** (1998) 159–185.

[19] W. M. Beltman: Viscothermal wave propagation including acousto-elastic interaction. Part I: Theory. J. Sound Vib. **227** (1999) 555–586.

[20] M. Malinen, M. Lyly, P. Råback, A. Kärkkäinen, L. Kärkkäinen: A finite element method for the modeling of thermo-viscous effects in acoustics. Proc. 4th European Congress on Computational Methods in Applied Sciences and Engineering ECCOMAS, Jyväskylä, Finland, 2004.

[21] W. M. Beltman, Y. H. Wijnant, M. J. Nijhof: An overview of models for viscothermal wave propagation, including fluid structure interaction. Proc. Acoustics'08 Paris, Acta Acustica united with Acustica, 94, 2008, 452.

[22] Comsol Multiphysics. http://www.comsol.com/products/.

[23] Elmer: Open source finite element software for multiphysial problems. available at http://www.csc.fi/elmer, 2007.

[24] O. Pironneau, F. Hecht et al.: freeFEM. available at http://www.freefem.org, 2005.

[25] A. Boufermel, N. Joly, P. Lotton: Numerical modeling of acoustic streaming in resonators. Proc. Acoustics'08 Paris, Acta Acustica united with Acustica **94** (2008).

[26] R. Bossart, N. Joly, M. Bruneau: Méthodes de modélisation numérique des champs acoustiques en fluide thermovisqueux. Proc. 6ème Congrès Français d'Acoustique, Lille, France, 2002, 411–414. available at http://hal.archives-ouvertes.fr/hal-00345808/fr/.

[27] F. Hecht: BAMG: Bidimensional anisotropic mesh generator. available at http://www-c.inria.fr/gamma/cdrom/www/bamg/eng.htm, 1997.

[28] P. Gentil: GRAME, Graphique mélina. available at http://perso.univ-rennes1.fr/pascal.gentil/programmes/grame/index.html, 2003.

[29] N. Joly: Finite element modeling of thermoviscous acoustics in closed cavities. Proc. Acoustics'08, Paris, Acta Acustica united with Acustica **94** (2008) 324. available at http://hal.archives-ouvertes.fr/hal-00346938/fr/.

[30] D. Marx, H. Bailliet, J.-C. Valière: Analysis of the acoustic flow at an abrupt change in section of an acoustic waveguide using particle image velocimetry and proper orthogonal decomposition. Acta Acustica united with Acustica **94** (2008) 54–65.

[31] P. Blanc-Benon, E. Besnoin, O. Knio: Experimental and computational visualization of the flow field in a thermoacoustic stack. C. R. Mecanique **311** (2003) 17–24.